Study of water wetting and water layer thickness in oil-water flow in horizontal pipes with different wettability

L.D. Paolinelli *, A. Rashedi, J. Yao, M. Singer

Institute for Corrosion and Multiphase Technology, Department of Chemical & Biomolecular Engineering, Ohio University, Athens, OH 45701, USA

HIGHLIGHTS

- Water wetting was studied in pipes with different wettability in oil-water flow.
- Pipe wettability plays a very important role in the oil wet to water wet transition.
- Droplet sticking and spreading are the main mechanisms for segregation in a hydrophilic pipe.
- Poor surface wettability hinders droplet sticking and spreading in a hydrophobic pipe.
- Segregation in a hydrophobic pipe occurs when local droplet accumulation is critical.

ARTICLE INFO

ABSTRACT

Two-phase oil-water pipe flow is common in oil production and transportation. Appropriate estimation of phase wetting (oil wet or water wet) of internal pipe walls can significantly reduce corrosion control costs, and increase confidence in measures taken to ensure the integrity of pipelines. Water wetting can be avoided by fully dispersing the water phase into the oil phase. It has been suggested that pipe wettability may affect oil-water flow patterns; particularly, water-in-oil dispersed flow transition boundaries. However, there are no systematic studies in the literature on this matter for carbon steel pipes, which are the preferable choice for economic reasons in the oil and gas industry. Moreover, traditional and widely used models to predict the onset of dispersed flow do not consider the effect of pipe wettability. This work studies phase wetting and water layer thickness in large scale oil-dominated oil-water horizontal flow in carbon steel and PVC pipes of similar internal diameter (0.1 m) and roughness, but different wettability. The effect of wetting hysteresis (oil or water pre-wetted pipe surface) on phase wetting is also investigated. It is demonstrated that pipe wettability plays a very important role on the transition boundaries for phase wetting (oil wet to water wet) and the transition to fully dispersed flow. Water droplet deposition and spreading are identified as the main mechanisms for incipient segregation in a hydrophilic pipe. In a hydrophobic pipe, poor surface wettability hinders the sticking and spreading of water droplets. Water wetting in a hydrophobic pipe requires a sufficient low flow velocity at which local droplet accumulation and coalescence becomes the dominant segregation mechanism. Predictions from available hydrodynamic models are compared with the experimental results and recommendations are provided.

© 2018 Elsevier Ltd. All rights reserved.

1. Introduction

Prediction of the phase wetting regime of internal pipe walls can be of paramount importance in industrial processes involving the flow of two immiscible liquids. For example, flow of liquid hydrocarbons and water is common in pipelines associated with oil production and transportation facilities. Contact between water and internal pipe walls can lead to serious corrosion problems when carbon steel is used (Kermani and Morshed, 2003; Pots et al., 2006; Smith and Joosten, 2006) as well as induce other problems, such as environmentally assisted cracking. This scenario is called water wetting (Cai et al., 2012; Pots et al., 2006). It is considered that under typical production conditions the hydrocarbon oil phase is not corrosive (Cai et al., 2012; Lotz et al., 1991). Since produced oils are generally less dense than produced water, the water tends to segregate and occupy the pipe bottom. However, if water is fully dispersed in oil (e.g., oil as continuous phase), water

* Corresponding author at: Institute for Corrosion and Multiphase Technology, Department of Chemical & Biomolecular Engineering, Ohio University, 342 W. State Street, Athens, OH 45701, USA.

E-mail address: paolinel@ohio.edu (L.D. Paolinelli).

Nomenclature

A	cross-sectional area of the pipe, m^2
C	droplet volumetric concentration, dimensionless
C_b	droplet volumetric concentration at the pipe bottom, dimensionless
C_D	droplet drag coefficient, dimensionless
C_m	constant for the estimation of mean droplet size, dimensionless
C_o	constant for the estimation of maximum droplet size, dimensionless
c'	radius of the adhesion patch of the attached sessile droplet, m
D	pipe diameter, m
d	droplet size, m
d_{crit}	critical droplet diameter, m
d_{cb}	critical droplet diameter from buoyancy criterion, m
$d_{c\sigma}$	critical droplet diameter from deformation criterion, m
d_{max}	maximum droplet diameter, m
$d_{max,o}$	maximum droplet diameter in diluted dispersion, m
d_{32}	Sauter mean droplet diameter, m
f	Fanning friction factor, dimensionless
g	gravitational acceleration, m/s^2
h	thickness of the water layer, m
h_0	average thickness of the water layer, m
h'	height of the attached sessile droplet, m
IP	phase inversion point, dimensionless
$I_1(K)$	modified Bessel function of order 1, dimensionless
K	parameter, $DU_s/2\varepsilon$, dimensionless
Ra	arithmetic surface roughness, m

Rz	average mean peak to valley distance of a roughness profile, m
Re_c	Reynolds number of the flow based on the continuous phase, dimensionless
Re_m	Reynolds number of the mixture flow, dimensionless
Re_p	Reynolds number of a settling droplet, dimensionless
r'	radius of the attached sessile droplet, m
U_c	continuous phase velocity, m/s
U_m	mixture velocity, m/s
U_s	droplet settling velocity, m/s
U_{sc}	superficial velocity of the continuous phase, m/s
U_{sd}	superficial velocity of the dispersed phase, m/s
y	vertical coordinate, m

Greek letters

β	pipe inclination angle from the horizontal, radians
ε	droplet turbulent diffusivity, m^2/s
ε_d	volumetric fraction of dispersed phase, dimensionless
ϵ	energy dissipation rate per unit of mass of the continuous phase, Watt/kg
ζ	dimensionless eddy diffusivity, dimensionless
θ	contact angle of the attached sessile droplet, radians
ρ_c	continuous phase density, kg/m^3
ρ_d	dispersed phase density, kg/m^3
ρ_m	mixture density, kg/m^3
μ_c	continuous phase viscosity, Pa s
μ_m	mixture viscosity, Pa s
σ	interfacial liquid-liquid tension, N/m

wetting can be avoided and corrosion occurrence becomes insignificant (Lotz et al., 1991). Full dispersion or entrainment of water into oil is only possible if the turbulent velocity fluctuations in the oil flow are sufficient to disrupt the water phase into droplets, keeping them suspended against gravity and preventing their accumulation and coalescence.

Appropriate knowledge of phase wetting can significantly reduce corrosion control costs as mitigation efforts can directly aim at the most critical pipeline areas where water wetting is likely to occur, as well as increase confidence in decisions taken to manage and ensure pipeline integrity. In this regard, several experimental studies have been performed to determine phase wetting regimes in oil-water pipe flow (Ayello et al., 2008; Cai et al., 2012; Kee et al., 2016; Paolinelli et al., 2017; Pots et al., 2006; Tang, 2011; Valle, 2000). Moreover, various efforts have been made on the quantification and modeling of water wetting phenomena (Cai et al., 2012; Pots et al., 2006; Pouraria et al., 2016; Tsahalis, 1977; Wicks and Fraser, 1975). Based on the information available in the literature, water wetting prediction has been suggested to be carried out using traditional models to predict the onset of liquid-liquid dispersed flow (NACE, 2008). These models, e.g., (Brauner, 2001; Torres et al., 2015; Trallero, 1995), assume that the flow is already dispersed and assess the balance between buoyancy forces and turbulent flow forces on dispersed phase droplets as criteria to determine if droplets will migrate towards the pipe bottom forming a separated fluid stream. Brauner (2001) also included an extra criterion as suggested by Barnea (1987), determining when dispersed phase droplets become excessively deformed and cannot be effectively dispersed. The aforementioned criteria only depend on fluids properties such as density, viscosity and interfacial tension; and the continuous phase turbulence intensity given by the flow rates of both fluids and the pipe geometry (e.g., diameter,

inclination and internal roughness). However, the effect of the wettability of the pipe surface is not considered.

Surface wettability has been suggested to play a role on flow patterns in oil-water pipe flow. Charles et al. (1961) studied two-phase flows with water and oils of similar density and different viscosity in a transparent plastic pipe of 0.026 m internal diameter (ID). They found that the oil with higher wetting affinity with the pipe wall was more likely to develop flow patterns where the oil formed the continuous phase. Hasson et al. (1970) studied flows of water and oil with almost similar density in glass pipes with different wetting properties (hydrophilic and hydrophobic) and 0.012 m ID. They observed that the pipe wetting properties had a strong influence on the stability of annular flow patterns, favoring annular films of water and hydrocarbon on the hydrophilic and hydrophobic pipes, respectively. Nädler and Mewes (1997) studied oil-water flows in a horizontal 0.059 m ID acrylic pipe. They mentioned, based on the findings of other researchers (Efthimiadu and Moore, 1994; Joseph et al., 1984), that the formation and type of emulsions produced from two immiscible liquids is influenced by the wetting properties of the experimental equipment. Therefore, it was suggested that the use of polymeric pipe in their experiments could favor wetting by the oil phase. Angeli and Hewitt studied pressure gradients (Angeli and Hewitt, 1999) and flow patterns (Angeli and Hewitt, 2000b) in horizontal oil-water flows with stainless steel and acrylic pipes of 0.024 m ID. The wetting of the steel was characterized by water-in-oil and oil-in-water contact angles, and found to be either hydrophobic or hydrophilic depending on the conditioning of the surface, i.e., if it was previously oil or water wetted, respectively. Conversely, the acrylic pipe was preferentially wetted by oil in all cases (Angeli and Hewitt, 1999). Under this circumstance, the authors found that, in the acrylic pipe, oil tended to remain as the continuous phase over a wider range of

flow conditions than in the steel pipe. They also pointed out that since acrylic pipes are widely used in experimental studies of liquid-liquid flows, care should be taken in applying the results of such experiments to practical cases where steel pipes are mostly used. Tang (2011) studied phase wetting in oil-water flows of different crude oils and a model oil in a 0.1 m ID flow loop with a carbon steel pipe section. He found that full entrainment of water in oil occurred at lower oil velocities for crude oil than for model oil. Moreover, he indicated that this behavior could not be fully explained by differences in the physicochemical properties of the oils such as density, viscosity and interfacial tension, and suggested the alteration of the wettability of the carbon steel pipe by contact with crude oil (e.g., from hydrophilic to hydrophobic) as an important factor. In this regard, it has been reported that compounds naturally present in crude oil, for example, aromatic hydrocarbons, nitrogen and sulfur containing compounds, and organic acids can adsorb onto carbon steel leading to hydrophobic surfaces (Aspenes et al., 2010; Ayello et al., 2013). Despite the fact that pipe surface wettability has been found to alter oil-water flow pattern transition boundaries, as far as the authors know, there are no systematic studies in the literature on this matter for carbon steel pipes, which are the preferable choice for economic reasons in the oil and gas industry.

The objective of this work is to study phase wetting, water layer thickness, and dispersed flow regime boundaries, in large scale oil-dominated oil-water horizontal flow in carbon steel and PVC pipes of similar internal diameter (0.1 m) and roughness, but different wettability. Flow tests using oil pre-wetted and water pre-wetted carbon steel pipe surfaces were performed to investigate the effect of surface wetting hysteresis (hydrophobic to hydrophilic) on phase wetting. Flow tests with PVC pipe were also performed to characterize phase wetting on a stable hydrophobic surface. The same oil and water fluids were used in all the experiments in order keep densities, viscosities and interfacial oil-water tension constant, while testing pipes with different wettability. Supplementary analyses of dispersed water droplet size and distribution, as well as water concentration at the pipe bottom, were also performed to better understand phase wetting results. It is demonstrated that pipe wettability plays a very important role on the phase wetting boundary (oil wet to water wet) in horizontal oil-water flow. The onset of water segregation is found to be different in hydrophilic and hydrophobic pipes. In addition, available hydrodynamic models are compared with experimental data and recommendations are provided.

2. Materials and methods

2.1. Wettability measurements

Wettability tests of the selected pipe materials were carried out using a goniometer consisting of two main parts; a test cell vessel and an image capture system. The vessel is made of stainless steel and has two aligned circular openings of 0.05 m diameter on its sides with flat glass windows for visual examination of the internal fluids without distorting droplet images, and a holder to place test specimens. The image capture system is composed of a monochrome digital camera with specialized optics and backlighting to enhance image illumination and contrast. The system is connected to a computer interface and takes pictures and video to assess the evolution of sessile droplets with time. Water droplets with a volume of about 8 μl were deposited on the test surfaces. Based on the radius of the non-deposited droplet, this corresponds to a Bond number of 0.06; this is low enough to avoid both shape distortion of the sessile droplet due to gravity and any error of measured contact angles (Srinivasan et al., 2011).

The surface of the carbon steel specimens was polished with 180-grit SiC paper, using water as a polishing fluid. The surface roughness was characterized using optical profilometry as 1.6 μm in terms of arithmetic roughness (Ra) and average mean peak to valley distance (Rz) of 14 μm. Two different procedures were used to prepare oil pre-wetted and water pre-wetted carbon steel surfaces for the wettability tests. The oil pre-wetted surface was obtained by washing the polished carbon steel with deionized water and then with isopropyl alcohol to remove water, and drying with cool air and finally immersing the sample in the hydrocarbon phase. On the other hand, the water pre-wetted surface was prepared by washing the polished carbon steel with deionized water and then with the test water, and by flushing the surface with a flow of hydrocarbon phase to thin the precursor water film prior to final immersion in the oil phase.

The PVC specimen was obtained by cutting a piece of a PVC pipe similar to the test section used in the multiphase flow experiments in order to assess the wettability of its internal surface as manufactured. The PVC specimen was washed with deionized water and isopropyl alcohol and dried with air prior to immersion in the hydrocarbon phase.

Contact angles of the sessile droplets were estimated by the truncated sphere method, where the droplet height (h') and contact base length ($2c'$) are measured from the digital images obtained in the tests using ImageJ® software:

$$\frac{c'}{h'} = \frac{\sin\theta}{1-\cos\theta} \tag{1}$$

where θ is the contact angle measured from inside of the sessile droplet as shown in Fig. 1.

2.2. Flow facility

Phase wetting and water layer thickness measurements in oil-water flow were performed using a large-scale fully inclinable multiphase flow loop. A schematic layout of the flow loop is shown in Fig. 2. The main part of the loop consists of a 30 m long, 0.1 m internal diameter (ID) flow line mounted on a steel rig structure. The loop consists of two parallel sections of pipes connected by a 180-degree bend. Oil and water are pumped separately from the individual storage tanks into the 0.1 m ID main line by progressive cavity pumps. Flow rates of oil and water are monitored independently by flow meters with an uncertainty of 10%. Water is injected into the main line at a T-junction through a 0.05 m ID secondary line. The fluid mixture first flows in a stainless steel pipe (upstream leg) over a distance equivalent to approximately 140 pipe diameters allowing flow to develop. The flow then enters a 1.8 m long test section where phase wetting and water layer thickness measurements are carried out. A clear acrylic section is located just
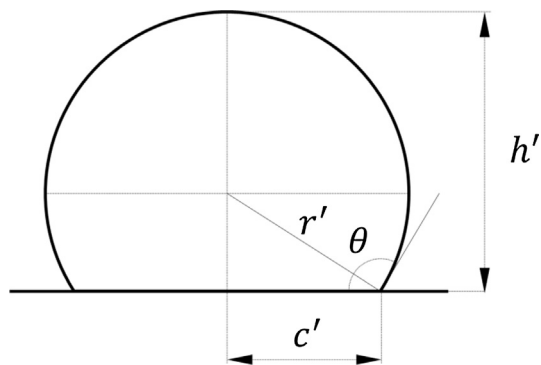

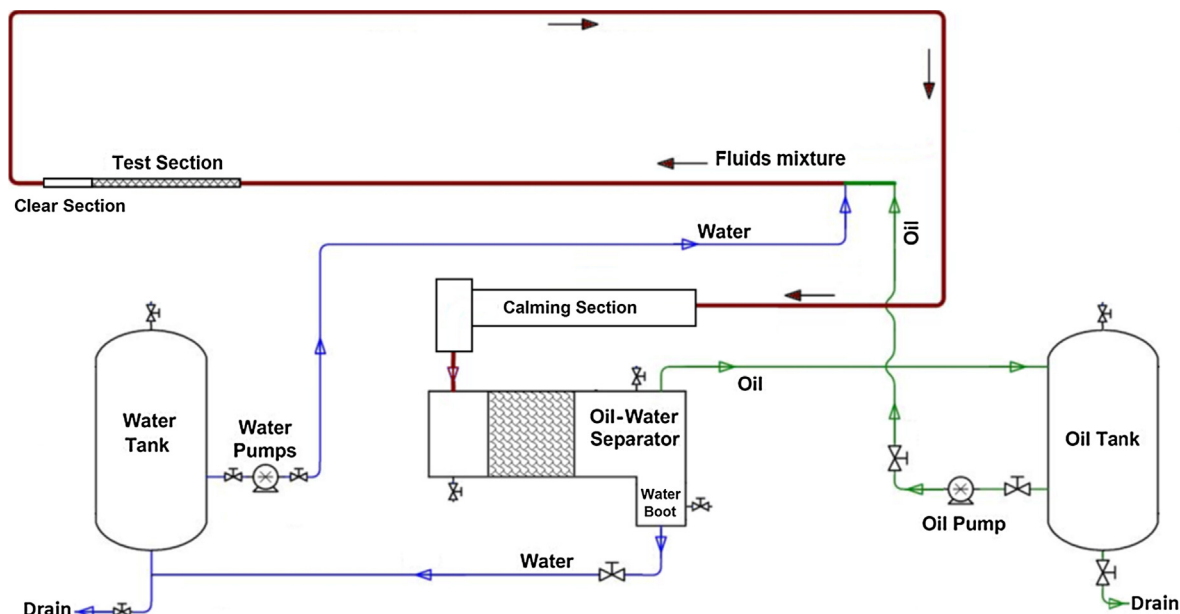**Fig. 1.** Two-dimensional drawing of the truncated sphere geometry.

Fig. 2. Schematic layout of the 0.1 m ID flow loop used for oil-water flow tests.

after the test section to allow visualization of the developed flow patterns. Upon exiting the main line, the mixture is directed to a calming section of 0.3 m ID and 7.5 m long for pre-separation of the oil and water and subsequently to an oil-water separator with mesh and plate droplet coalescers; this equipment is described elsewhere (Cai et al., 2012). The separated oil and water streams are then returned to their respective storage tanks, made of stainless steel and with a capacity of 2 m³, for further recirculation.

2.3. Flow loop test section and instrumentation

Phase wetting tests in oil-water flow were performed using two test sections of identical geometry, 0.1 m ID and 1.8 m long (Fig. 3), one made of carbon steel and the other one made of PVC. Phase wetting regime and thickness of developed water layers were measured using a concentric two-electrode high frequency (HF) impedance probe, as shown in Fig. 4a. The probe with an inner carbon steel electrode of 12.5 mm diameter ($2r_i$) and an outer stainless steel electrode of 25 mm diameter ($2r_o$) was used flush-mounted at the pipe bottom where water is most likely to segregate, as indicated in Fig. 4b, at a distance of about 16 pipe diameters downstream from the inlet of the test section. The width of both electrodes (w) is 3 mm. This configuration was used to measure phase wetting and water layer thickness in oil-water pipe flow in previous work (Paolinelli et al., 2017). The probe was operated with an AC voltage of 10 mV rms and frequency of 20 kHz using

a Gamry REF 600® potentiostat with a computer interface. Once the desired flow conditions were stabilized, the impedance measurements were performed continuously for at least 2 min, using a sampling period of approximately 0.5 s. The presence of water layers in contact with the probe, and their thickness, was determined from the measured impedance values (modulus and phase angle) in relation to the theoretical response of the probe and the electrical conductivity of the water phase, as reported elsewhere (Paolinelli et al., 2017). The probe can detect water layers as thin as 0.003 mm on average. The uncertainty of the measurement of water layer thickness is estimated as lower than 20%, considering the error of impedance measurements from the potentiostat and variations in water conductivity due to temperature fluctuations.

Prior to introducing the impedance probe in the test section, its exposed surface was polished with a 240 grit SiC paper, in the presence of deionized water, in a special device to assure the proper shape of the internal pipe curvature, and later alignment. The probe was also rinsed with deionized water and isopropanol, then dried with a clean cloth, and subsequently flush-mounted at the bottom of the test section. The misalignment of the probe surface with respect to the test section surface was always less than 0.1 mm.

A sampling port of 9 mm ID located at the bottom of the test section (Fig. 3) was used to obtain fluid samples during the flow tests. The port was directly connected to a ball valve that was fully open when sampling. This allowed the maximum suction possible
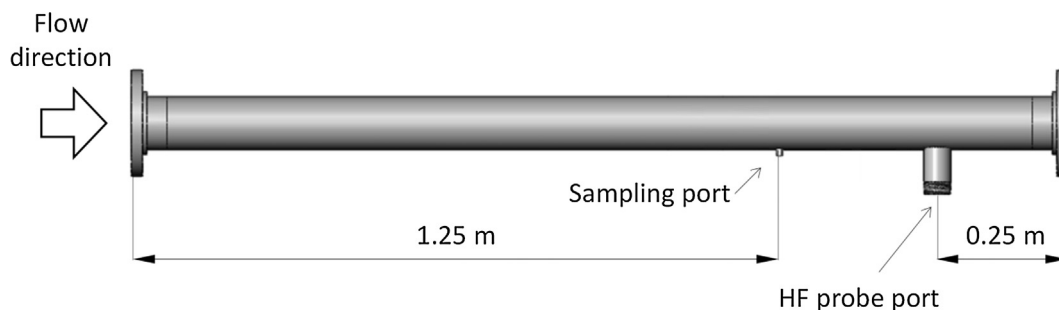

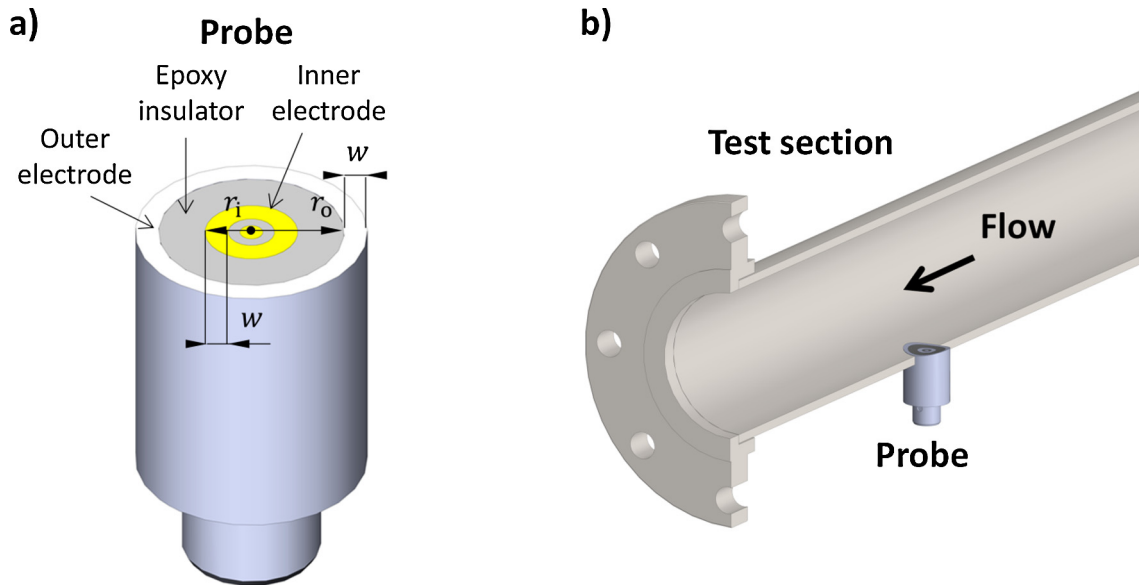**Fig. 3.** Schematic of the test section used for phase wetting measurements.

Fig. 4. (a) Schematic of the impedance probe; (b) Cut view of the test section with the flush-mounted probe.

to overcome the inertia of dispersed water droplets flowing in the pipe direction and obtain representative samples of the oil-water mixture close to the pipe wall. For each tested condition, once the flow was stable, at least two fluid samples of about 25 ml were pulled into transparent graduated cylindrical containers that were stored standing in special holders overnight to allow the complete separation of the oil and water by gravity. It is worth mentioning that the model oil and brine used in this work separate rapidly and do not require centrifugation. The volumetric amount of water in each sample was assessed directly by reading the total sample volume, and the water volume on the graduated scale of the container. The error of the measurement method is estimated as 10%.

Before each experimental run with the carbon steel test section, its internal surface was polished using a rotating flexible abrasive tool (180 grit) with deionized water as the polishing fluid. The surface was then washed with deionized water and isopropanol, then dried with a clean cloth. The roughness of the polished test section surface was indirectly measured using optical profilometry, generated data being taken from the surface of an epoxy-mounted specimen with an area of about 5 cm^2 of the internal pipe wall. The obtained roughness values were $Ra = 1.7$ μm and $Rz = 10$ μm. Each experimental run consisted of two sets of flow conditions. The first one corresponded to the tests for the oil pre-wetted carbon steel pipe where the polished test section was first put in contact with oil at the highest available superficial velocity, then the water was injected at the desired water cut and surface wetting was measured. Subsequently, the oil superficial velocity was reduced to its next value maintaining the water cut, and the process was repeated until reaching the lowest used mixture velocity (0.7 m/s) where consistent water wetting of the pipe bottom was monitored. The second set of flow conditions corresponded to the tests for the water pre-wetted carbon steel pipe where the mixture velocity was gradually increased, maintaining the desired water cut until reaching the maximum available value. Once the experimental run was completed for the given water cut, the flow loop was drained and the test section and the impedance probe surfaces were re-conditioned to test a different water cut.

The internal roughness of the PVC test section was measured as $Ra = 1$ μm and $Rz = 7.5$ μm. The surface of the PVC pipe was washed with deionized water and isopropanol and dried with a clean cloth before starting the flow tests, which consisted of 2–3

experimental runs as described above. The flow loop was then drained and the test section surface was cleaned and the impedance probe surface was reconditioned for the subsequent experimental runs.

2.4. Droplet size measurements

Water droplet sizes generated in the oil-water flow were measured from pictures of the flow taken from the side and the bottom of the flow loop clear section. This allowed more comprehensive characterization of the droplet size distribution without missing the larger droplets that usually occupy the pipe bottom. A digital camera of 4912 × 3264 pixels of resolution and 1/4000 s of shutter speed was employed. The optical focus of the camera was always at the pipe wall at halfway of the pipe width, with a maximum depth of field of approximately 50 mm. An illuminated white screen was used as background to enhance visualization. A schematic of the setup used to image flow characteristics in the clear section is shown in Fig. 5.
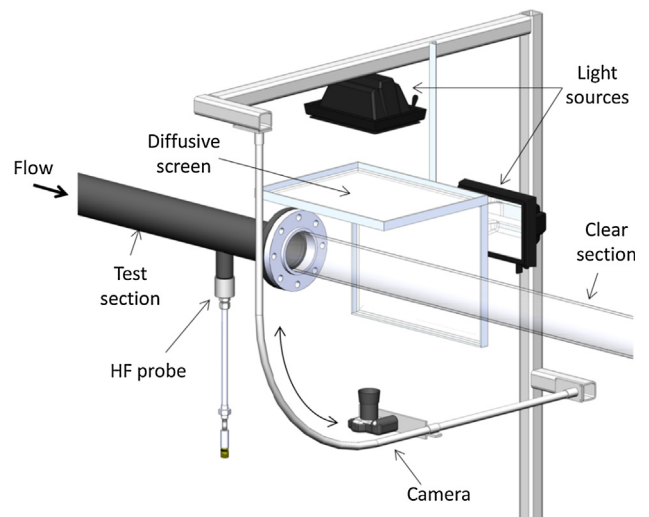

Fig. 5. Schematic of the setup used to image flow characteristics.

No device, such as a liquid filled box, was used to diminish the optical distortion produced by the transparent pipe curvature. Instead, the effect of optical distortion was characterized by placing Teflon® spheres of calibrated diameter ($d = 4.7$ mm and $d = 6.3$ mm) at different positions at the cross-section of the clear pipe filled with test oil, in order to simulate the presence of water droplets. Pictures of the calibrated spheres were taken with the same setup as for the flow experiments, for a total of 18 positions distributed in an equal-spaced grid comprising half of the pipe cross-section area. The assessment showed that only particles located at a distance from the focal plane of about 50 mm or less were sharp enough to be measured. The maximum optical distortion ($e_{opt} = 100(d_{measured} - d)/d, \%$) was found for particles located just at the top or bottom of pipe walls, referred to as side view, where they became almost non-visible. Conversely, optical distortion was found to be within an acceptable range of ±7% for particles placed at distances smaller than 3/4 of the external pipe radius from the pipe center, including the error of the measurement procedure due to image size calibration. Therefore, only droplets located inside this visual field and seen with a sharp contour were considered.

Since droplets can present oval contours due to their deformation by inertial, flow or gravity forces, and also optical distortion from the used setup, a mean droplet size was characterized as: $d = \sqrt{d_1 d_2}$, where d_1 and d_2 are the largest and the smallest droplet axial lengths, respectively. Droplet measurement was performed manually using ImageJ® software to measure characteristic sizes from the obtained digital pictures. A minimum sample count of 600 droplets was used to determine droplet size distribution for each analyzed condition. The variability of the manual measurement process was found to be below 15% for maximum and average droplet size by comparing the results from two different operators for at least 3 different experimental conditions.

Mean droplet size was characterized from the measured droplet size distributions in terms of Sauter mean diameter:

$$d_{32} = \frac{\sum d_i^3 n_i}{\sum d_i^2 n_i} \tag{2}$$

where n_i is the number of droplets of size d_i.

The residual water content of the oil after the oil-water separator was measured by taking fluid samples from the bottom of the line exiting the separator. The procedures for fluid sampling and water content measurement were the same as those described in Section 2.3. It was found that for mixture flow rates below 0.016 m³/s (mixture velocity of 2 m/s), the residual water content was less than 1.5% of the injected water cut value. For higher mixture flow rates, the residual water content ranged from 1.5% to less than 5% of the injected water cut value. The recirculation of residual water, due to the incomplete separation of small droplets (with estimated diameters below about 1 mm), could have affected, to some extent, the measured droplet size distributions. Nevertheless, this contamination does not significantly modify the measured droplet size distributions and mean droplet sizes as further shown in Section 3.3.

2.5. Test fluids and flow conditions

Isopar V®, a clear saturated paraffinic hydrocarbon, was used as the oil phase. The water phase was 1 wt% NaCl solution prepared from deionized water. The properties of the test fluids are listed in Table 1. The oil-water inversion point is indicated as water volumetric concentration. It was measured in a stirred vessel using high frequency conductance measurements with a parallel-rod two-electrode setup.

Table 1
List of properties of the test fluids (values at 25 °C).

Property	Oil	Water
Density (kg/m³)	810	1005
Dynamic viscosity (Pa s)	0.009	0.001
Oil-water interfacial tension (N/m)	0.049	
Oil-water inversion point (%)	25	

The use of a conductive electrolyte as water phase (1.76 S/m) helps prevent significant local conductivity changes when the solution comes in contact with the carbon steel test section, which may corrode and release iron ions.

Flow experiments were performed in horizontal condition at room temperature (~25 °C) using mixture velocities from 0.7 to 4 m/s and water cuts from 1% to 20%.

3. Results and discussion

3.1. Wettability of the employed pipe materials

Fig. 6 shows water-in-oil contact angles as a function of time measured on carbon steel surfaces pre-wetted by oil and water, and PVC surfaces. Oil pre-wetted carbon steel shows hydrophobicity (contact angle ~145°) at the first second after contact with a water droplet. Then, contact angle gradually decreases becoming hydrophilic after about 1 min, reaching a value of about 75° after 10 min (Fig. 7a). On the other hand, water droplets spread very rapidly and collapse on water pre-wetted carbon steel surfaces showing zero contact angle. The wetting hysteresis seen on carbon steel would be related to the water-liking nature of its surface due to the preferential adsorption of water molecules compared to oil. It is interesting to note that water droplets take a considerable time (about a minute) to spread and displace the hydrocarbon towards a hydrophilic equilibrium in water-free oil pre-wetted carbon steel surface. However, once water adsorbs on the carbon steel surface (water pre-wetted), even after thoroughly flushing with hydrocarbon phase as in the present case, a thin water film still remains attached on surface leading to a super hydrophilic surface. PVC surfaces show hydrophobic behavior with contact angles of about 170° at the first seconds after droplet contact, stabilizing at about 130° for longer times (Fig. 7b).

3.2. Phase wetting and water layer thickness in oil-water flow with different pipe wettability

It is worth repeating that, in the case of oil pre-wetted carbon steel pipe (OCS), flow tests were performed for each water cut going from the highest available mixture velocity to lower velocities (e.g., 0.7 m/s), until obtaining a consistent water wet regime. Thereafter, the pipe surface was reconditioned for the next set of experimental runs with different water content. Water pre-wetted carbon steel pipe (WCS) tests were performed starting from a low mixture velocity at water wet regime to the highest mixture velocity available, attempting to reach the full oil wet regime. The tests performed with PVC pipe showed similar phase wetting regimes and water layer thicknesses when mixture velocities were changed from low to high and vice versa.

Fig. 8 shows the phase wetting regimes and time-averaged water layer thickness measured at the pipe bottom for WCS, OCS and PVC pipe surfaces as function of operating conditions. The map shows areas with no data at the upper right corner due to the limitation of the flow rig to deliver larger water flow rates. The results had good reproducibility in terms of phase wetting regime and water layer thickness (e.g., 20% on average) between
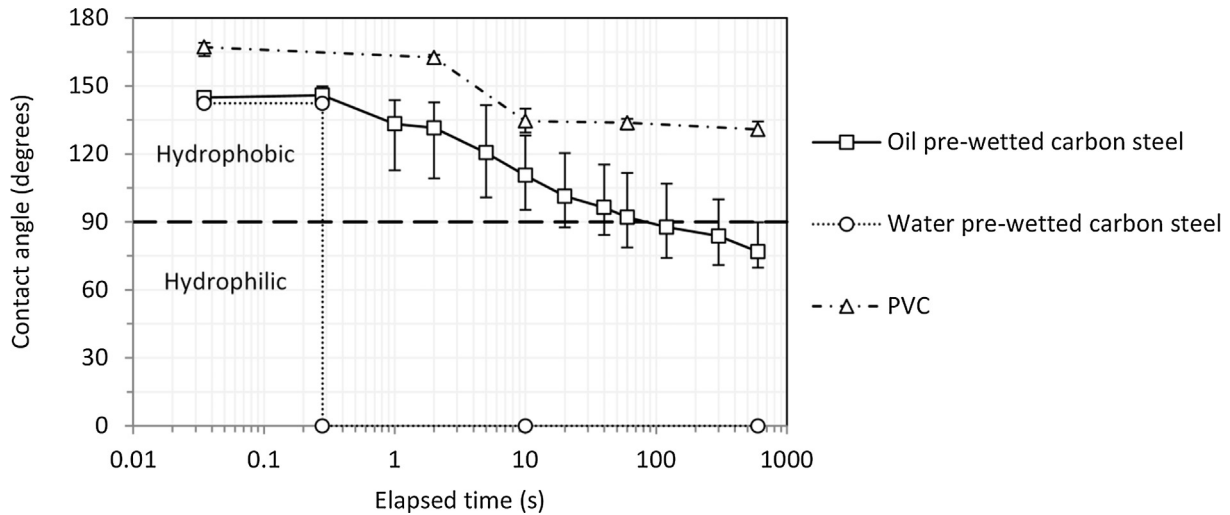
Fig. 6. Water-in-oil contact angle in function of time for carbon steel surfaces pre-wetted by oil and water and for PVC surface.
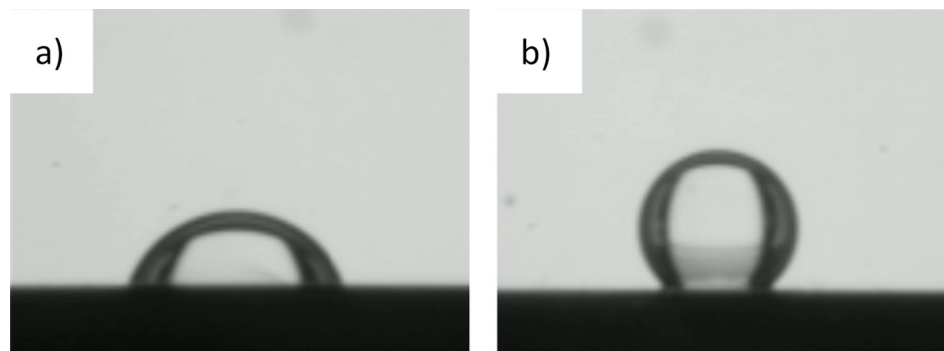

Fig. 7. Examples of water-in-oil contact angles after 10 min of contact on: (a) oil pre-wetted carbon steel surface; (b) PVC surface.

2 separate experimental runs with the same flow conditions. The phase-wetting regimes are characterized as "full oil wet" (red[1] circles), where only oil was detected, or water wet where water was detected; the data is further arranged in ranges to illustrate the variation of water layer thickness (e.g., hollow green triangles indicate average water layer thicknesses between 0.1 mm and 0.5 mm).

It is obvious from the measurements that critical mixture velocities to obtain full oil wet regime are significantly affected by the pipe surface wettability. For PVC pipe, mixture velocities of 1.3 m/s and 2 m/s are enough to obtain a full oil wet regime for water cuts of 1% and 5%, respectively. On the other hand, the OCS pipe requires mixture velocities of 2 m/s and 2.3 m/s for full oil wet regime for water cuts of 1% and 5%, respectively. The WCS pipe shows full oil wet regime at mixture velocities of 2.3 m/s and 3 m/s only for water cuts of 1% and 2% since very thin water layers (<0.1 mm) are detected for larger water cuts even at mixture velocities above 3 m/s. Somewhat similar behavior was found by Angeli and Hewitt (2000b), however, they did not characterize the effect of oil pre-wetted or water pre-wetted surfaces on oil-water flow in a steel pipe.

Irrespective of the pipe wettability, larger mixture velocities are needed to overcome water wetting or the formation of water layers of considerable thickness (for example, >0.5 mm) at the pipe bottom when water cut increases. This is in line with the findings of other works specific to phase wetting (Cai et al., 2012; Kee et al.,

2016), and flow patterns where fully dispersed water-in-oil regimes were studied (Angeli and Hewitt, 2000b; Lovick and Angeli, 2004; Nädler and Mewes, 1997; Perera et al., 2017; Trallero et al., 1997; Vielma et al., 2008).

Fig. 9 shows examples of water layer thickness (h) measured at the bottom of the WCS pipe as function of time for oil-water flow with different mixture velocities and 5% water cut. The uncertainty in the measured water layer thickness values is lower than 20%, as mentioned above. However, error bars are not provided in Fig. 9 to enable easier visualization of water layer thickness behavior with time. Time-averaged water layer thickness values (h_0) of approximately 4.5 mm, 3.7 mm, 0.8 mm, 0.14 mm, 0.06 mm and 0.05 mm were estimated for mixture velocities of 1 m/s, 1.5 m/s, 2 m/s, 2.5, 3 m/s and 4 m/s, respectively; as listed in Table 2. Table 2 also lists the rms value of the fluctuations of the water layer thickness ($h - h_0$) and its value relative to the average thickness (h_0). In general, the amplitude of the fluctuations tends to increase when the thickness of the water layer increases. On the other hand, the values of the fluctuations relative to the average water layer thickness tend to increase when the water layer thickness decreases. This effect is related to the larger relative effect of mass gain or loss by incorporation or entrainment of water droplets in thinner water layers with less volume.

These thin water layers at the bottom of the WCS pipe are developed at mixture flow velocities where the PVC pipe is fully oil wet. Visual observation of the oil-water flow at a clear section immediately downstream of the WCS and PVC test sections show that flow patterns in the different pipes are, at first glance, similar,

---

[1] For interpretation of color in Fig. 8, the reader is referred to the web version of this article.
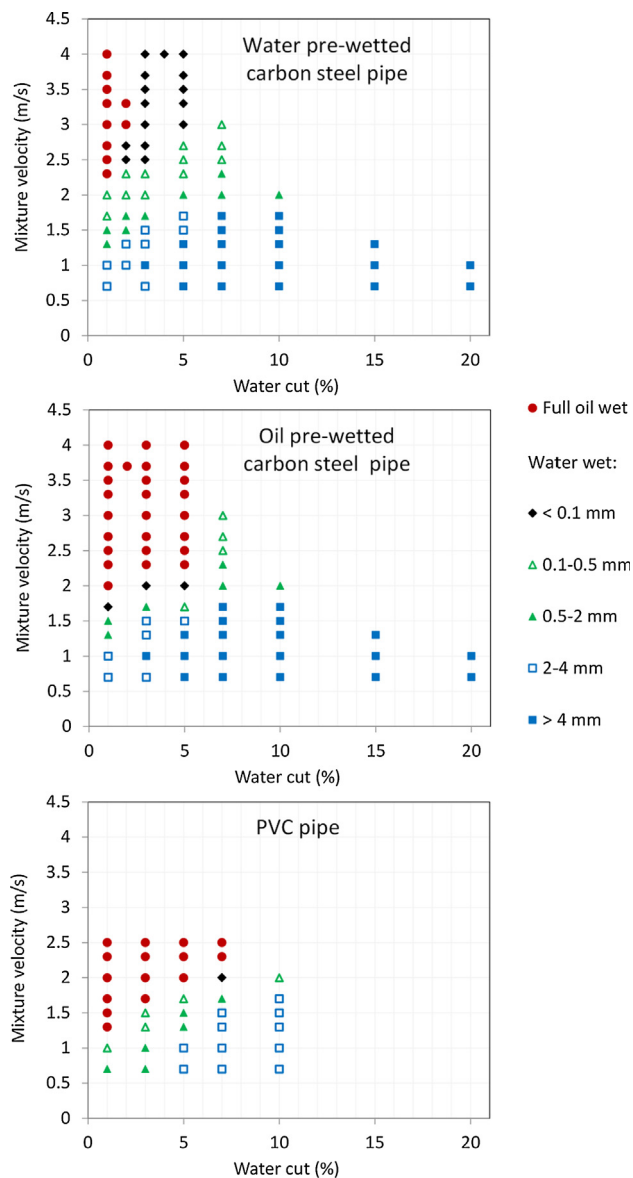
Fig. 8. Phase wetting regime and time-averaged water layer thickness at the pipe bottom in function of operating conditions in oil-water horizontal flow in 0.1 m ID pipes of different material and surface wettability.

about 1 min to a value of around 0.01 mm and stays somewhat stable. Then, water injection is resumed and the water layer thickness rapidly grows in a few seconds stabilizing again at its original average thickness of about 0.02 mm. The thickness of the water layer depends on the droplet deposition and entrainment rates, which are similar when the layer thickness stabilizes. It is worth noting that after interrupting the water injection, the water layer is not completely removed by the bulk oil flow with an elapsed time of about 3 min. This is unsurprising considering that full dewetting of the water phase by the oil flow is very unlikely on hydrophilic surfaces (contact angle close to zero), according to experimental observations and hydrodynamic models for dewetting reported elsewhere (Eggers, 2004; Redon et al., 1991). Moreover, the shearing and tearing of the water layer into droplets by the inertial forces of the oil flow may be limited if its thickness is very small. Therefore, the removal of the water layer may take significant time and also may be impeded by surface roughness irregularities, as shown in previous studies of liquid film removal in tubes by flow of an immiscible fluid (Mickaily and Middleman, 1993; Yan et al., 1997).

Conversely to what is seen in a hydrophilic pipe, hydrophobic pipe walls such as PVC lead to poor or even no attachment of sinking water droplets allowing their re-entrainment by the oil flow. This phenomenon occurs at mixture flow velocities where the droplet concentration at the pipe bottom is still low enough to prevent significant accumulation and coalescence to produce major phase segregation. It is interesting to note that the OCS pipe, which is transiently hydrophobic, shows critical mixture velocities for full oil wet regime somewhat larger than the PVC pipe for water cuts up to 5%. However, as seen in Fig. 8, no transition to the full oil wet regime is found for larger water cuts such as 7%, similar to the WCS pipe for the same flow conditions. This is related to the fact that the OCS surface becomes overwhelmed by droplet/wall collisions, which are more frequent in denser dispersions, leading to droplet spreading and altering the metastable hydrophobic nature of the surface to hydrophilic.

3.3. Water droplet sizes in dispersed oil-water flow with different pipe wettability

This section studies water droplet sizes that were measured from dispersed flow pictures taken at the side and bottom of a clear section just downstream of the WCS and PVC test sections. The goal is to determine if the differences seen in phase wetting regimes measured in the different pipe materials are related or not with variations in produced droplet sizes. Measurements were performed for mixture velocities of 2.5 m/s or lower where the maximum shutter speed of the photographic camera facilitated acquisition of sharp and clear images of water droplets. Only flow conditions where water was observed as fully entrained were analyzed. This limited the available set of data for comparison between the WCS and PVC pipes to water cuts up to 3% and mixture velocities between 2 m/s and 2.5 m/s; larger water cuts as well as lower mixture velocities showed visible water streams at the bottom of the clear section downstream from the WCS pipe.

Figs. 12 and 13 show maximum water droplet size (d_{max}) and mean droplet size (d_{32}) for dispersed oil-water flow with different mixture velocities and 1% and 3% water cut, respectively. The vertical error bars account for the maximum uncertainty linked to the droplet measurement procedure, that is estimated as ±7% due to visual processing error (i.e., picture sharpness and clearness) plus ±7.5% due to variability found from different operators. The horizontal error bars account for the uncertainty of the mixture velocity values of ±5%. Maximum and mean droplet sizes show

as seen in Fig. 10. However, even when the water phase seems to be fully dispersed as in the case of mixture velocity of 2 m/s in Fig. 10, water layers of less than 0.5 mm thickness are measured at the bottom of the WCS pipe. The formation of these layers would be related to the deposition of water droplets that contact the pipe wall due to gravity even when hydrodynamic dispersive forces of the oil phase are significant. Colliding water droplets are very prone to stick onto the hydrophilic carbon steel surface, subsequently forming water streams that do not grow much in thickness due to the shearing action of the continuous phase flow. In order to confirm the aforementioned hypothesis, the formation of thin water layers was monitored in situ by HF impedance as show in the example in Fig. 11, where water injection was interrupted in a dispersed oil-water flow and then resumed to observe the evolution of the developed water layer. A relatively stable water layer of about 0.02 mm thickness is formed under constant flow conditions (mixture velocity of 3.7 m/s and 3% water cut). When water injection is interrupted, the thickness of the water layer decreases in
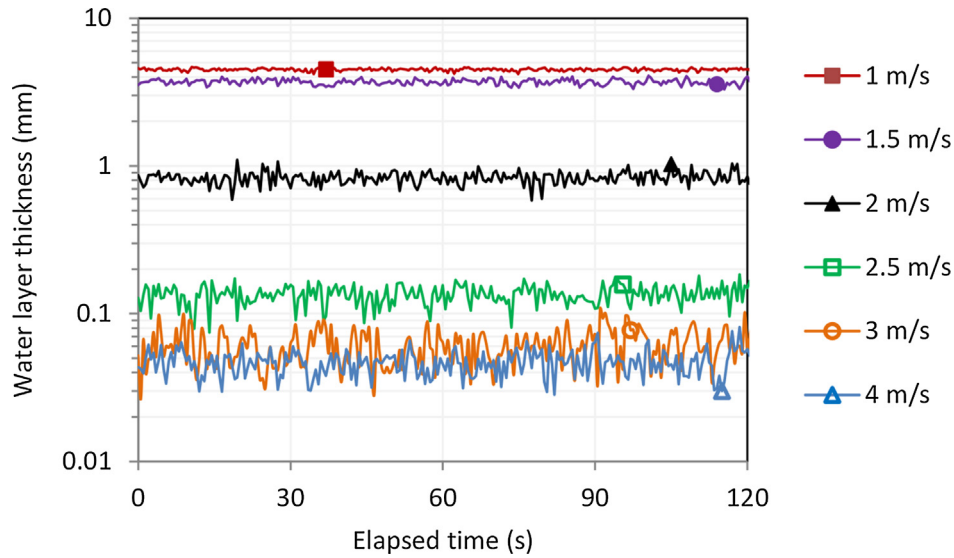
Fig. 9. Water layer thickness at the WCS pipe bottom in function of time, estimated from HF impedance measurements in horizontal oil-water flows with different mixture velocities and 5% water cut.
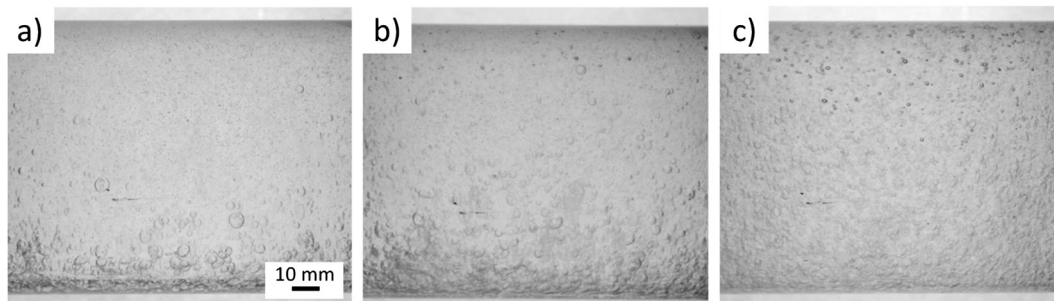
Table 2
Time-averaged water layer thickness and rms values of its fluctuations for horizontal oil-water flows with different mixture velocities and 5% water cut.

Mixture velocity (m/s)	h_0 (mm)	$(h - h_0)_{rms}$ (mm)	$(h - h_0)_{rms}/h_0$ (%)
1	4.5	0.09	2
1.5	3.7	0.15	4.3
2	0.83	0.081	9.7
2.5	0.14	0.02	14
3	0.063	0.016	25
4	0.047	0.009	19

differences below 20% and 11%; respectively, between the WCS and PVC test sections. These relatively small differences would indicate that droplet sizes in the WCS and PVC test sections are similar, which can be also inferred from the examples of droplet size distributions shown in Fig. 14. This differs from the observations of Angeli and Hewitt (2000a) that reported that the pipe material influenced significantly the drop size distributions, with smaller drop sizes in a stainless steel pipe than in an acrylic pipe.

The present results are unsurprising since droplet size in turbulent fully dispersed flow is expected to be controlled by the mean

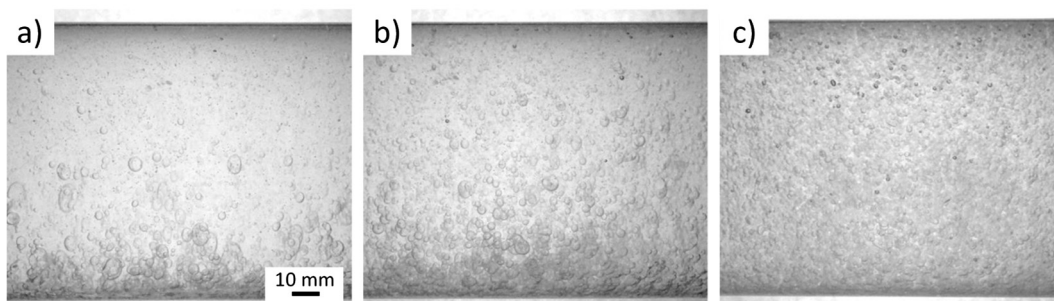## Water pre-wetted carbon steel pipe

PVC pipe

Fig. 10. Example of flow patterns visualized from the side of a clear section after a WCS pipe (top) and after a PVC pipe (bottom) for horizontal oil-water flows with 3% water cut and mixture velocity of: (a) 1.3 m/s, (b) 1.5 m/s, (c) 2 m/s.
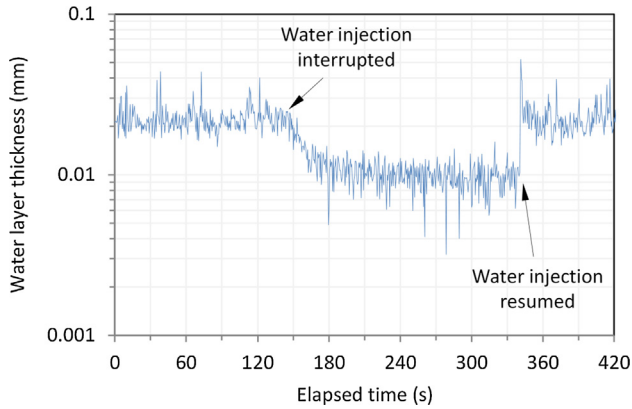
Fig. 11. Example of the evolution with time of the thickness of thin water layers formed at the bottom of the WCS in horizontal oil-water flow with different mixture velocities of 3.7 m/s and 3% water cut.
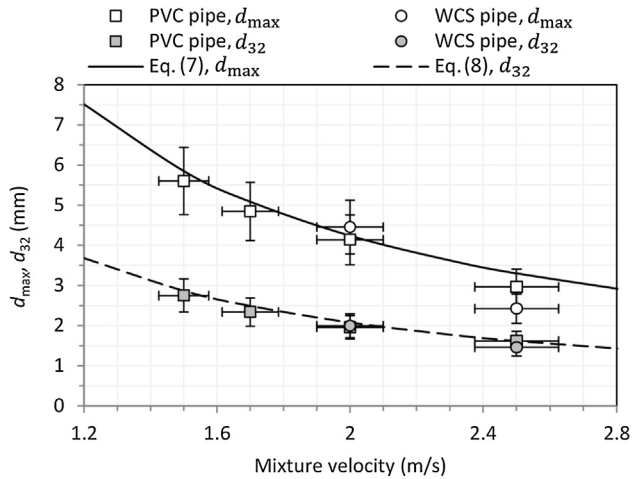

Fig. 12. Maximum and mean water droplet sizes in function of the mixture velocity for 1% water cut in horizontal oil-water flow just downstream from the WCS and PVC test sections.

Fig. 13. Maximum and mean water droplet sizes in function of the mixture velocity for 3% water cut in horizontal oil-water flow just downstream from the WCS and PVC test sections.
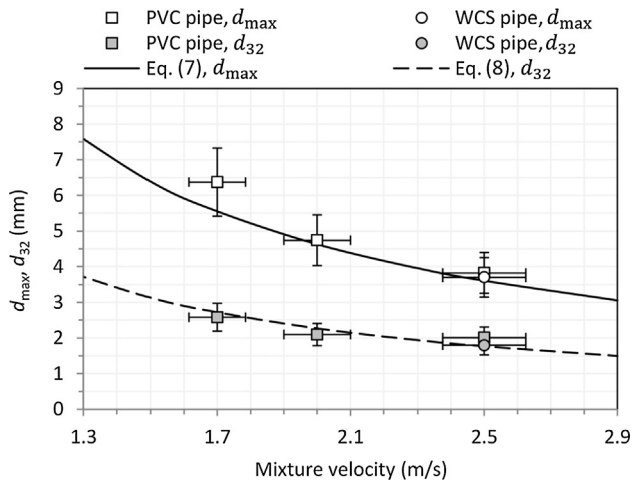
energy dissipation rate in the continuous phase (Hinze, 1955; Kostoglou and Karabelas, 2005), which for pipe flow is:

$$\epsilon = \frac{2\rho_m f\, U_c^3}{D\rho_c(1-\varepsilon_d)} \quad (3)$$

where D is the pipe diameter, f is the Fanning friction factor of the oil-water mixture flow, ρ_m is the density of the oil-water mixture, and ε_d is the volumetric fraction of dispersed phase, which is considered similar to the water cut in horizontal dispersed flow, assuming no slip between the oil and water phases:

$$\varepsilon_d = \frac{U_{sd}}{U_{sd}+U_{sc}} \quad (4)$$

where U_{sd} is the superficial velocity of the dispersed phase, and U_{sc} is the superficial velocity of the continuous phase. The continuous phase velocity (U_c) is considered to be almost equal to the mixture velocity ($U_c \cong U_m$), which is by definition the sum of U_{sd} and U_{sc}. Since the WCS and PVC pipes are both hydraulically smooth due to their relatively small internal roughness, the friction and therefore the mean energy dissipation rate are similar for the same flow conditions.

The measured droplet size distributions were fitted with a log-normal statistical function. The fit is excellent as seen in Fig. 14, with a coefficient of determination (R^2) larger than 0.997 for all cases. The standard deviation of the fitted log-normal distributions (σ_{LN}) was similar for all tested flow conditions with an average value of 1.37 with a standard deviation of 5.8%. In this circumstance, a minimum of at least 3 droplets with sizes equal or larger than d_{95} (size associated to 95% of the cumulative droplet volume) can be found in the total number of 600 droplet counts measured per flow condition.

As mentioned in Section 2.4, small residual water contents were found in the oil after the oil-water separator. In order to account for this effect, the measured droplet size distributions and the associated mean droplet sizes were recalculated by removing the volume fraction identified as contamination from the smaller droplet size population. Based on the measured residual water contents, the "contaminating" volume fraction was assumed conservatively to be 1.5% and 5% of the injected water volume for mixture flow rates below and above 0.016 m³/s (mixture velocity of 2 m/s), respectively. The recalculated mean droplet sizes increase less than 3% compared to the mean droplet sizes calculated from the "unfiltered" distributions. The "filtered" droplet size distributions were also fitted with a log-normal function showing excellent agreement in all cases (R^2 >0.997). The standard deviation values of the fitted log-normal distributions (σ_{LN}) were again similar for all tested flow conditions with almost the same average value and dispersion (1.36 ± 0.08) as for the "unfiltered" distributions.

The actual contamination of the clean oil stream with residual water may have been smaller than the values measured at the exit of the oil-water separator, since some of the unseparated water could have settled at the oil tank bottom before recirculation. Unfortunately, this cannot be confirmed since no sampling port was available for fluid sampling at the oil injection line. Given the small differences found between droplet size distributions and mean droplet sizes calculated with and without considering residual water, the effect of contamination by recirculated water droplets on the results shown in Figs. 12, 13 and 14 is considered negligible.

It must be pointed out that the used optical measurement method mostly gives information on droplet sizes near the pipe wall where the droplet concentration is, for example, higher than at other locations towards the center of the pipe cross-section. Therefore, the measured water droplet distributions may have a larger uncertainty than reported when it comes to represent the behavior of the entire cross-section.
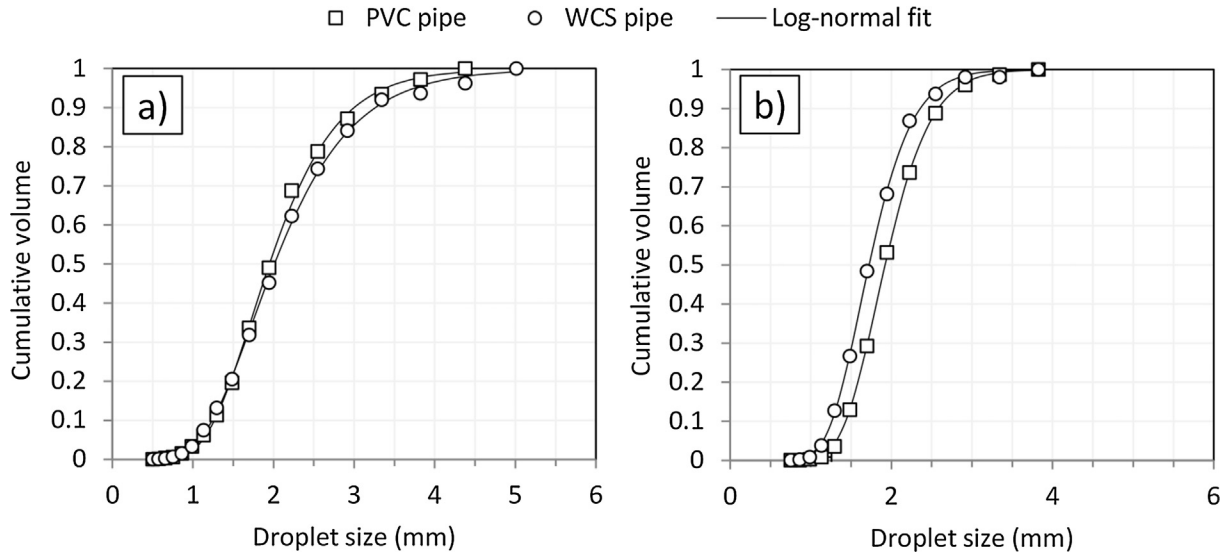
Fig. 14. Water droplet size distributions just downstream from the WCS and PVC test sections in horizontal oil-water flow: (a) Mixture velocity 2 m/s and 1% water cut, (b) Mixture velocity 2.5 m/s and 3% water cut.

In order to model water droplet sizes, Hinze's approach is used to obtain maximum droplet size in dilute dispersion (Hinze, 1955):

$$d_{max,o} = C_o \left(\frac{\sigma}{\rho_c}\right)^{3/5} \epsilon^{-2/5} \qquad (5)$$

where σ is the oil-water surface tension, ρ_c is the density of the oil, and C_o is a constant determined by Hinze as 0.725 from the best fit of available experimental data. Eq. (5) is valid providing that (Brauner, 2001; Kubie and Gardner, 1977):

$$\left(\frac{\mu_c^3 \epsilon}{\rho_c^3}\right)^{1/4} \ll d_{max,o} < 0.1D \qquad (6)$$

where μ_c is the dynamic viscosity of the continuous phase. It is worth mentioning that the dependency of maximum droplet size on the parameters shown in Eq. (5) has been confirmed using realistic functions for frequency and probability of turbulent droplet break-up in dispersed liquid-liquid flow and population balance analysis (Kostoglou and Karabelas, 2005).

To account for the effect of the volumetric fraction of dispersed phase on maximum droplet size, the dilute size $d_{max,o}$ is modified by the factor suggested by Mlynek and Resnick (1972); then, this gives the maximum droplet size as:

$$d_{max} = d_{max,o}(1 + 5.4\epsilon_d) \qquad (7)$$

A least squares method was used to find the best fit for the available experimental data with Eqs. (5) and (7) where the value of the constant C_o was determined as 1.39. The modeled d_{max} values are plotted in Figs. 12 and 13 as solid lines, the average and maximum absolute errors with the experimental data are about 8% and 27%. The mean droplet size is found to be proportional to the maximum droplet size:

$$d_{32} = C_m d_{max} \qquad (8)$$

where C_m was determined to be 0.49 with a standard deviation of 7%. The modeled d_{32} values are plotted in Figs. 12 and 13 as dashed lines, the average and maximum absolute errors with the experimental data are about 6% and 14%. Similar d_{32}/d_{max} ratios of 0.45 and 0.39 were found by Angeli and Hewitt (2000a) and Karabelas (1978) in oil-water horizontal pipe flow, respectively.

The maximum and mean measured droplet sizes are well correlated with the classical dependency of a $-2/5$ exponential power

of the mean energy dissipation rate for inertial turbulent break-up. The maximum droplet sizes are about 2 times larger than predictions from the widely used Hinze model (Eq. (5) with $C_o = 0.725$). Similar findings were reported elsewhere for liquid-liquid pipe flow (Angeli and Hewitt, 2000a; Karabelas, 1978; Sleicher, 1962). Differences found in maximum and mean droplet sizes characterized among the various works available in the literature, and the attainment (or not) of steady state droplet sizes in pipe flow are well discussed and theoretically justified in the works of Kostoglou and Karabelas (1998, 2005).

3.4. Comparison of the phase wetting data with available hydrodynamic models

As mentioned above, this section is dedicated to the comparison of the experimental phase wetting regime data with known hydrodynamic criteria for the onset of fully dispersed flow. These models assume that the flow is already fully dispersed and they assess its stability against the segregation of the dispersed phase.

Brauner (2001) proposed that the transition to dispersed flow pattern takes place when the continuous phase turbulence is sufficiently intense to break the dispersed phase into droplets smaller than the critical size (d_{crit}) with the transitional criterion:

$$d_{max} \leqslant d_{crit} \qquad (9)$$

provided that the continuous phase flow is turbulent $Re_c \geqslant 2100$, where $Re_c = \rho_c D U_c / \mu_c$.

The critical droplet diameter required in Eq. (9) is estimated as:

$$d_{crit} = Min(d_{cb}, d_{c\sigma}) \qquad (10)$$

Here d_{cb} is the maximum droplet size above which droplets will migrate to the pipe wall:

$$d_{cb} = \frac{3}{8} \frac{\rho_c f U_c^2}{(\rho_d - \rho_c)Dg \cos\beta} \qquad (11)$$

where β is the pipe inclination angle from the horizontal, g is the gravitational acceleration, and ρ_d is the density of the dispersed phase. Eq. (11) equates the gravity force and the turbulent flow force on the droplet in the radial direction of the pipe; it has been used elsewhere (Trallero, 1995; Trallero et al., 1997) as single criterion to determine the transition to dispersed flow in oil-water flow.

The parameter $d_{c\sigma}$ is the maximum droplet diameter above which droplets deform significantly from their spherical shape mainly due to gravity, and turbulent flow forces are no longer effective to fully disperse droplets and avoid their contact with the bottom pipe wall:

$$d_{c\sigma} = \left[\frac{0.4\sigma}{(\rho_d - \rho_c)g\cos\beta'} \right]^{1/2} \tag{12}$$

where $\beta' = |\beta|$ when $|\beta|$ is below 45°.

The friction factor of the mixture flow is estimated using the Blasius correlation:

$$f = 0.046Re_m^{-0.2} \tag{13}$$

where $Re_m = \rho_m D U_m / \mu_m$. The density of the oil-water mixture is estimated as:

$$\rho_m = \varepsilon_d \rho_d + (1 - \varepsilon_d)\rho_c \tag{14}$$

and the mixture viscosity, μ_m, is considered similar to the viscosity of the continuous phase ($\mu_m \cong \mu_c$) as assumed by other authors from pressure drop experimental data obtained in model mineral oil and water pipe flow (Elseth, 2001; Utvik et al., 2001).

Fig. 15 shows the transitional criteria described by Eqs. (9–12) in the phase wetting maps for the WCS, OCS and PVC. In this analysis, d_{max} is calculated using Eq. (7) shown in the previous section. It must be noticed that the criterion $d_{max} \leqslant d_{c\sigma}$ (solid line), which is dominant over the criterion $d_{max} \leqslant d_{cb}$ (dashed line), describes fairly well the critical mixture velocities for the full oil wet transition for water cuts lower than 3% in the hydrophilic WCS pipe. This criterion also coincides with the transition to very small water layer thickness (< 0.1 mm) at the pipe bottom for the available data at larger water cuts. In the case of the OCS and PVC pipes, the criterion $d_{max} \leqslant d_{c\sigma}$ greatly overestimates the full oil wet transition. Although the criterion $d_{max} \leqslant d_{cb}$ seems to match the full oil wet transition in the OCS pipe for water cuts below 7%, it fails to describe the behavior at larger water cuts; moreover, it does not correlate well with the full oil wet transition data for PVC pipe.

Both criteria $d_{max} \leqslant d_{c\sigma}$ and $d_{max} \leqslant d_{cb}$, grouped in Eq. (10) attempt to estimate the onset where dispersed phase droplets are prone to contact the pipe wall. This is explicit in the concept of d_{cb}, and is implicit in $d_{c\sigma}$ where Brauner (2001) and Barnea (1987) introduced Eq. (12) based on an expression reported by Brodkey (1967). Brodkey estimated when drag forces on droplets deviate from solid-like behavior due to shape distortion, producing swerving motion. Brauner (2001) stated that Eq. (10) yields complete transitional criteria to dispersed flow; however, this may not be true in some cases. If dispersed phase droplets contact a hydrophobic non-adherent pipe wall, they are unlikely to effectively stick, spread and form segregated streams. Contrarily, contacting droplets would be re-entrained by the continuous phase boundary layer flow and fully dispersed flow regime would be maintained. Under this circumstance, criteria in Eq. (10) is no longer valid to determine dispersion onset, and accumulation and coalescence of droplets at the pipe bottom may be a better criterion to define the transition boundary for fully dispersed flow, as suggested by Pots et al. (2006). For water-in-oil dispersions in horizontal pipe flow, if water droplet concentration at the pipe bottom (C_b) is large enough to reach a critical concentration where droplets are no longer stable and coalesce; for example, at a concentration similar to the phase inversion point (IP), the formation of a water stream is inevitable. Consequently, to avoid accumulation and coalescence of dispersed droplets at the pipe bottom the following relationship should be satisfied:
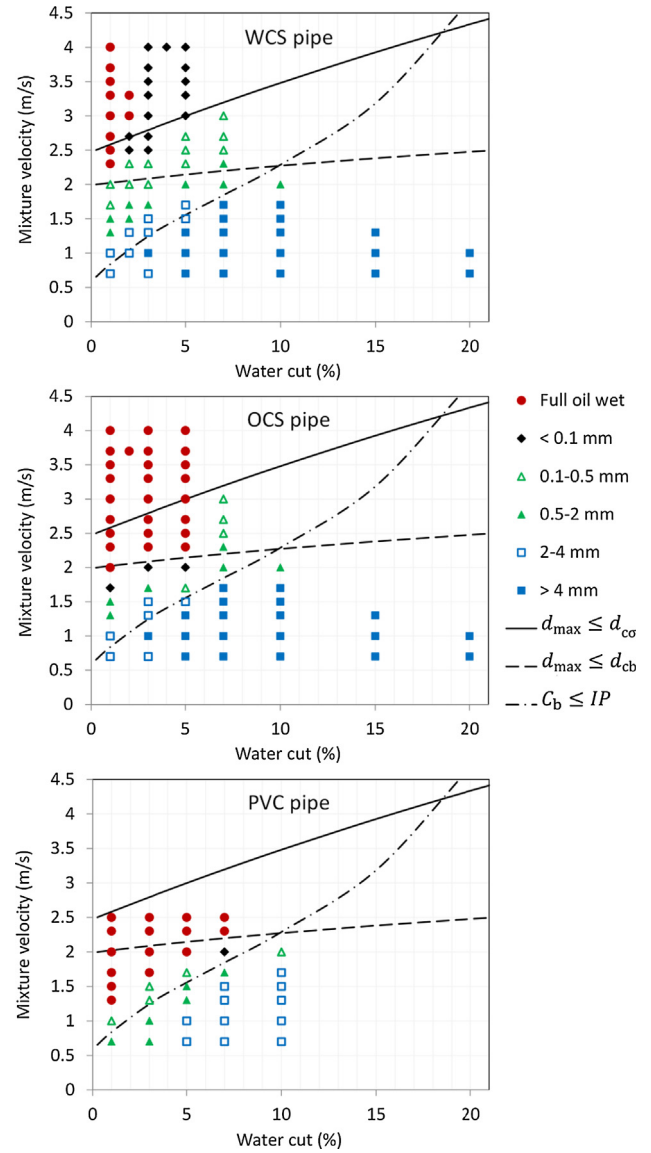
$$C_b < IP \tag{15}$$

Fig. 15. Comparison of dispersed flow criteria with maps of phase wetting regime and time-averaged water layer thickness at the pipe bottom for oil-water horizontal flow in 0.1 m ID pipes of different material and surface wettability.

An approximation of the droplet concentration across the pipe section can be made by using the transport (advection-diffusion) equation as reported elsewhere (Karabelas, 1977; Segev, 1984). Assuming steady state and considering the mass balance of the dispersed droplets and continuous phase fluxes, Karabelas proposed the following equation for horizontal flow (Karabelas, 1977):

$$U_s C(1 - C) - \varepsilon \frac{\partial C}{\partial y} = 0 \tag{16}$$

where C is the droplet volumetric concentration, ε is the droplet turbulent diffusivity that is assumed to be constant across the pipe section and is estimated as:

$$\varepsilon = \zeta \frac{D}{2} \sqrt{\frac{\rho_m f}{2\rho_c}} U_m \tag{17}$$

where ζ is the dimensionless eddy diffusivity that can be considered as constant with a value of 0.255 (Karabelas, 1977); and U_s is the settling velocity of the mean droplet size:

$$U_s = \sqrt{\frac{4}{3} \frac{d_{32}|\rho_d - \rho_c|g}{\rho_c C_D}} \qquad (18)$$

where C_D is the droplet drag coefficient, which can be approximated with the Schiller-Naumann (Schiller and Naumann, 1933) correlation (solid spheres):

$$C_D = \frac{24}{Re_p}(1 + 0.15Re_p^{0.687}) \qquad (19)$$

where $Re_p = \rho_c d_{32} U_s/\mu_c$, with $Re_p < 1000$.

Eq. (16) neglects the effect of hydrodynamic forces near the wall such as Saffman type forces. Droplet concentration is assumed to vary only with the vertical coordinate ($C(y)$), and the total droplet mass remains constant across the pipe section ($\int C(y)dA = \varepsilon_d A$). Besides, droplets do not adhere to the pipe surface and droplet sizes do not vary with time. Although expression (16) was developed for dilute dispersions, it has successfully been used to predict the concentration profile of dispersed particles in solid–liquid pipe flow with solid volume concentrations as high as 20% (Kaushal et al., 2002). A more complicated integro-differential version of Eq. (16) for multiple droplet sizes is available elsewhere (Karabelas, 1977). Although using the droplet size distribution can be more accurate than using a single mean droplet size representing the entire droplet population (Segev, 1984), for the sake of simplicity we will make use of the latter.

In the present case, droplet concentration at the pipe bottom is approximated using the closed-form solution of Eq. (16) suggested by Karabelas (1977):

$$C_b = \left[1 + 2\frac{(1 - \varepsilon_d)}{\varepsilon_d} \frac{I_1(K)}{K} \exp(-K)\right]^{-1} \qquad (20)$$

where:

$$K = \frac{DU_s}{2\varepsilon} \qquad (21)$$

and $I_1(K)$ is the modified Bessel function of order 1 (truncated at the sixth term):

$$I_1(K) = \frac{1}{2}K\left[1 + \frac{K^2}{8} + \frac{K^4}{192} + \frac{K^6}{9216} + \frac{K^8}{737280} + \frac{K^{10}}{88473600}\right] \qquad (22)$$

Although the series in Eq. (22) is valid for K values lower than 1.5 (Abramowitz and Stegun, 1964), it was found to provide a good approximation for K values as high as 4, overestimating the droplet concentration at the pipe bottom to less than 10% when using Eq. (20) with respect to the numerical solution of Eq. (16).

Fig. 15 shows the critical mixture velocities calculated with the criterion $C_b \leqslant IP$ as dash-dot lines. The value of phase inversion point (IP) of the mineral oil and brine used in the flow experiments was found to be about 0.25 (Table 1). This value is somewhat close to the value of 0.34 calculated using the mechanistic model proposed by Brauner and Ullmann (2002). Eq. (15) describes very well the transition to fully dispersed flow, and so the full oil wet regime over the available range of experimental data for the hydrophobic PVC pipe. This would confirm the aforementioned hypothesis that sticking of water droplets is not effective in hydrophobic pipes when turbulent forces are not enough to prevent droplets from contacting the pipe wall (Eq. (9) is not satisfied). Instead, accumulation of water droplets at the pipe bottom exceeding the inversion point is the dominant criterion to assess the stability of fully dispersed flow. Note that this modeling approach, where the oil-water mixture is assumed to be already fully dispersed, matches well the experimental transitions from fully dispersed to segregated flow and vice versa, which are found to be similar in the PVC pipe.
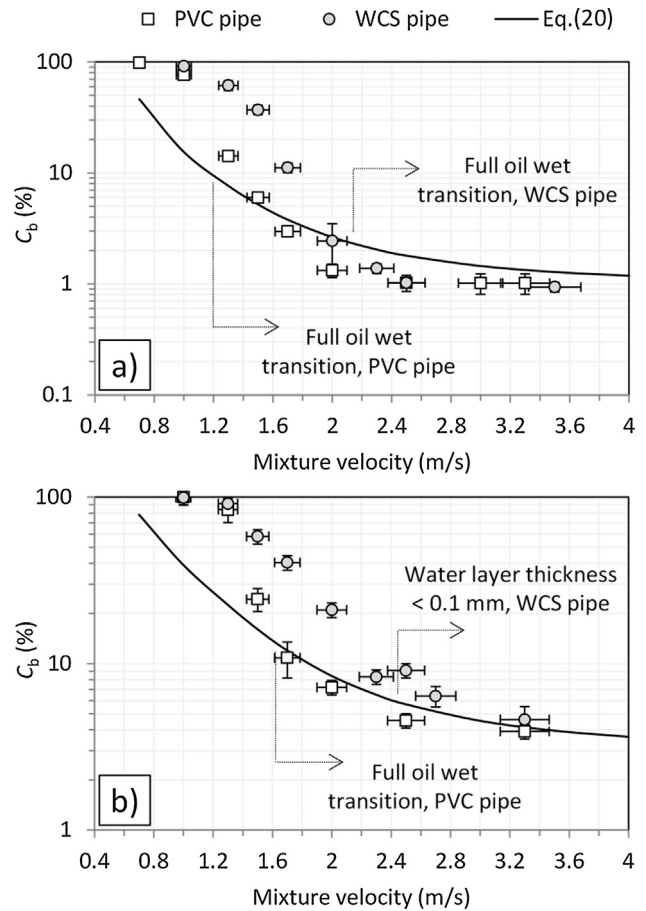

Fig. 16. Water concentration at the bottom of the WCS and PVC test sections in function of the mixture velocity in oil-water horizontal flow with: (a) 1% water cut, (b) 3% water cut.

Fig. 16 shows examples of measured water concentration at the bottom of the WCS and PVC test sections as a function of the mixture velocity for water cuts of 1% and 3%. Water concentration measured at the pipe bottom increases as mixture velocity decreases. This is due to water droplet accumulation and/or water segregation; the latter can lead to concentrations as high as 100%. It is worth noting that Eq. (20) describes fairly well the water concentration at the bottom of both pipes when the oil-water flow is fully dispersed (mixture velocities above the experimental full oil wet transition shown in Fig. 15). This is particularly true for the hydrophobic PVC test section where a larger range of experimental data of fully dispersed flow is available; for mixture velocities below the full oil wet transition, the measured water concentration is higher than predictions from Eq. (20). In the case of the PVC pipe, this would be due to the fact that a critical droplet concentration is reached at the bottom and water droplets massively coalesce forming segregated water streams. This critical droplet concentration may indeed be associated with the phase inversion point (IP) as proposed in Eq. (15). For example, the measured water concentration in Fig. 16 significantly increases and detaches, from Eq. (20), at values above 14%–24% (for flows with 1% and 3% water cut, respectively), which are close to the measured IP of 25%. On the other hand, the water concentration measured at the bottom of the hydrophilic WCS pipe increases and separates from Eq. (20) at, for example, values as low as 2.5% for flows with 1% water cut, just at a mixture velocity value similar to the experimental full oil wet transition. This would be related to the formation of segregated water layers due to droplet deposition and spreading as shown

above in Section 3.2, which occurs even if the concentration of dispersed droplets near wall is certainly low. It is worth mentioning that when water layers segregated at the pipe bottom become very thin (i.e., <0.1 mm), as in the case of flows with 3% water cut and mixture velocities above 2.4 m/s, water concentration values measured at the pipe bottom are larger than but still close to those based on Eq. (20).

3.5. General considerations

It has been shown that wettability of the internal pipe surface can greatly alter phase wetting regime (oil wet or water wet) and the onset for full dispersion in large scale oil-dominated two-phase oil-water flow. The onset of fully dispersed flow and oil wet regime occurs at significantly larger mixture velocities in a hydrophilic pipe (e.g., WCS) than in a hydrophobic pipe (e.g., PVC). The available evidence indicates that differences seen between hydrophilic and hydrophobic pipe surfaces are related to the ability of water droplets to stick and spread on the pipe wall, or not, as the case may be.

Carbon steel can show metastable hydrophobicity or extreme hydrophilicity according to the fluid that first contacts the surface, be it mineral oil or water, respectively. This wetting hysteresis leads then to significant variation of phase wetting regimes in oil-water pipe flow; particularly, for low water cuts (<7%). If the carbon steel surface is hydrophilic, deposition and spreading of water droplets at the pipe bottom is likely to occur even at mixture velocities as high as 4 m/s; developing thin water layers that may or may not pose an integrity risk. From this point of view, the history of a pipeline in terms of which fluid wetted first its surface (oil or water) would be important when assessing the likelihood of water segregation. Practically speaking, this is impossible to determine in industrial applications due to the broad range of operating conditions and eventual upsets throughout the lifetime of pipeline facilities. On the other hand, if very thin water films (e.g., <0.1 mm thickness) are formed in carbon steel pipes, they might be rapidly saturated with ferrous ions from corrosion due to their large surface/volume ratio and limited replenishment promoting the formation of protective corrosion product layers that reduce metal dissolution rates to below acceptable values (Kermani and Morshed, 2003; Nešić, 2007; Smith and Joosten, 2006). In general, as mentioned in the introduction section, natural components of crude oil can alter carbon steel surface making it hydrophobic (Aspenes et al., 2010; Ayello et al., 2013; Richter et al., 2014). In this context, a carbon steel pipe may behave similarly to, for example, a PVC pipe where water droplets are unlikely to stick and spread and fully dispersed flow can be maintained at lower mixture velocities, which represents a great advantage for the point of view of integrity management. Unfortunately, chemical composition of crude oil can be very different among reservoirs, and so its effect on the surface wettability of carbon steel is variable; this is in almost all cases unknown to pipeline operators.

When it comes to predicting phase wetting regime, the widely adopted criteria introduced by Brauner were assessed. It is worth reminding that a more realistic estimation of maximum dispersed droplet size was used based on modifying Hinze's equation in this work. Brauner's model seems to describe fairly well the threshold where major droplet deposition and subsequent water segregation occurs in hydrophilic pipe. However, it dramatically overpredicts the onset of water dropout in a hydrophobic pipe. Instead, a criterion that considers droplet accumulation and coalescence at the pipe bottom is more appropriate in this case. It is worth mentioning that the presence of surface active agents, either natural or artificially added to the oil-water mixture, can greatly affect the water distribution. For example, stiff emulsions can form with or without

a remaining water layer at the bottom. This is seen in the field, but it is almost impossible to address via a model.

More work should be done to better understand the formation and evolution of segregated thin films or rivulets in oil-water flow, which is a topic that has been barely addressed in the literature. These are complex phenomena where interfacial forces between liquids and between the liquids and the solid pipe wall can become dominant over viscous and inertial forces due to flow. Multiple interactions occur between colliding droplets and attached droplets or already formed liquid streams. Moreover, droplet detachment from the formed liquid stream occurs simultaneously. Good understanding and modeling of these problems would help to enhance the prediction of the onset for fully dispersed flow; in particular, in pipes where wettability favors sticking and spreading of colliding droplets.

In general, hydrophobic polymer pipes are used in experimental multiphase flow studies, attempting to mimic industrial applications where carbon steel is the most used pipe material. Given the present findings, it is strongly recommended to use representative pipe material when studying flow phenomena that may be affected by pipe surface wetting characteristics.

4. Conclusions

- The phase wetting regime (oil wet or water wet) and the onset of fully dispersed water-in-oil horizontal flow can be greatly affected by the water wettability of internal pipe surface. For example, the onset of fully dispersed flow occurs at significantly larger mixture velocities in a hydrophilic pipe (e.g., water pre-wetted carbon steel) than in a hydrophobic pipe (e.g., PVC).
- Carbon steel shows metastable hydrophobicity or extreme hydrophilicity according to the fluid that first contacts the surface, be it model mineral oil or water, respectively. This wetting hysteresis leads to significant variation of phase wetting regimes; particularly, for low water cuts (<7%).
- Water droplet deposition and spreading are identified as the main mechanisms for the onset of water segregation in a hydrophilic pipe. In a hydrophobic pipe, poor surface wettability hampers the sticking and spreading of water droplets. Water wetting in a hydrophobic pipe requires a sufficient low flow velocity at which local droplet accumulation and coalescence becomes the prevailing segregation mechanism.
- Pipe surface wettability does not significantly affect water droplet size distribution in fully dispersed flow. The maximum and mean measured droplet sizes can be well correlated with classical models of inertial turbulent break-up with a dependency of a − 2/5 exponential power of the mean energy dissipation rate.
- When predicting the onset of fully dispersed flow, the widely adopted criteria introduced by Brauner describes fairly well the threshold where major droplet deposition and subsequent water segregation occurs in a hydrophilic pipe, providing an adequate droplet size calculation is used. However, it dramatically overpredicts the onset of water dropout in hydrophobic pipe. Instead, a criterion that estimates droplet accumulation at the pipe bottom sufficient to reach a critical concentration for major droplet coalescence (e.g., the phase inversion point) is found to describe very well the transition from fully dispersed to segregated flow in a hydrophobic pipe.

References

Abramowitz, M., Stegun, I.A., 1964. Handbook of Mathematical Functions With Formulas, Graphs, and Mathematical Tables, National Bureau of Standards, Applied Mathematics Series 55, US Department of Commerce, Washintong D.C.

Angeli, P., Hewitt, G.F., 1999. Pressure gradient in horizontal liquid–liquid flows. Int. J. Multiph. Flow 24, 1183–1203.

Angeli, P., Hewitt, G.F., 2000a. Drop size distributions in horizontal oil-water dispersed flows. Chem. Eng. Sci. 55, 3133–3143.

Angeli, P., Hewitt, G.F., 2000b. Flow structure in horizontal oil-water flow. Int. J. Multiph. Flow 26, 1117–1140.

Aspenes, G., Dieker, L.E., Aman, Z.M., Høiland, S., Sum, A.K., Koh, C.A., Sloan, E.D., 2010. Adhesion force between cyclopentane hydrates and solid surface materials. J. Colloid Interface Sci. 343, 529–536.

Ayello, F., Li, C., Tang, X., Cai, J., Nesic, S., Cruz, C.I.T., Al-Khamis, J.N., 2008. Determination of Phase Wetting in Oil-Water Pipe Flows, NACE Corrosion 2008. NACE International, Houston, TX, Paper, p. 8566.

Ayello, F., Robbins, W., Richter, S., Nesic, S., 2013. Model compound study of the mitigative effect of crude oil on pipeline corrosion. Corrosion 69, 286–296.

Barnea, D., 1987. A unified model for predicting flow-pattern transitions for the whole range of pipe inclinations. Int. J. Multiph. Flow 13, 1–12.

Brauner, N., 2001. The prediction of dispersed flows boundaries in liquid–liquid and gas–liquid systems. Int. J. Multiph. Flow 27, 885–910.

Brauner, N., Ullmann, A., 2002. Modeling of phase inversion phenomenon in two-phase pipe flows. Int. J. Multiph. Flow 28, 1177–1204.

Brodkey, R.S., 1967. The Phenomena of Fluid Motions. Dover Publications, INC., NY.

Cai, J., Li, C., Tang, X., Ayello, F., Richter, S., Nesic, S., 2012. Experimental study of water wetting in oil-water two phase flow—Horizontal flow of model oil. Chem. Eng. Sci. 73, 334–344.

Charles, M.E., Govier, G.W., Hodgson, G.W., 1961. The horizontal pipeline flow of equal density oil-water mixtures. Canadian J. Chem. Eng. 39, 27–36.

Efthimiadu, I., Moore, I.P.T., 1994. Phase inversion of liquid—liquid dispersions produced between parallel shearing plates. Chem. Eng. Sci. 49, 1439–1449.

Eggers, J., 2004. Hydrodynamic theory of forced dewetting. Phys. Rev. Lett. 93, 094502.

Elseth, G., 2001. An Experimental Study of Oil/Water Flow in Horizontal Pipes. PhD thesis, Department of Technology. The Norwegian University of Science and Technology, Porsgrunn, Norway.

Hasson, D., Mann, V., Nir, A., 1970. Annular flow of two immiscible liquids I. Mechanisms. Canadian J. Chem. Eng. 48, 514–520.

Hinze, J.O., 1955. Fundamentals of the hydrodynamic mechanism of splitting in dispersion processes. AIChE J. 1, 289–295.

Joseph, D.D., Nguyen, K., Beavers, G.S., 1984. Non-uniqueness and stability of the configuration of flow of immiscible fluids with different viscosities. J. Fluid Mech. 141, 319–345.

Karabelas, A.J., 1977. Vertical distribution of dilute suspensions in turbulent pipe flow. AIChE J. 23, 426–434.

Karabelas, A.J., 1978. Droplet size spectra generated in turbulent pipe flow of dilute liquid/liquid dispersions. AIChE J. 24, 170–180.

Kaushal, D.R., Tomita, Y., Dighade, R.R., 2002. Concentration at the pipe bottom at deposition velocity for transportation of commercial slurries through pipeline. Powder Technol. 125, 89–101.

Kee, K.E., Richter, S., Babic, M., Nešić, S., 2016. Experimental study of oil-water flow patterns in a large diameter flow loop—the effect on water wetting and corrosion. Corrosion 72, 569–582.

Kermani, M.B., Morshed, A., 2003. Carbon dioxide corrosion in oil and gas production - a compendium. Corrosion 59, 659–683.

Kostoglou, M., Karabelas, A.J., 1998. On the attainment of steady state in turbulent pipe flow of dilute dispersions. Chem. Eng. Sci. 53, 505–513.

Kostoglou, M., Karabelas, A.J., 2005. Toward a unified framework for the derivation of breakage functions based on the statistical theory of turbulence. Chem. Eng. Sci. 60, 6584–6595.

Kubie, J., Gardner, G.C., 1977. Drop sizes and drop dispersion in straight horizontal tubes and in helical coils. Chem. Eng. Sci. 32, 195–202.

Lotz, U., Bodegom, L.v., Ouwehand, C., 1991. The effect of type of oil or gas condensate on carbonic acid corrosion. Corrosion 47, 636–645.

Lovick, J., Angeli, P., 2004. Experimental studies on the dual continuous flow pattern in oil-water flows. Int. J. Multiph. Flow 30, 139–157.

Mickaily, E.S., Middleman, S., 1993. Hydrodynamic cleaning of a viscous film from the inside of a long tube. AIChE J. 39, 885–893.

Mlynek, Y., Resnick, W., 1972. Drop sizes in an agitated liquid-liquid system. AIChE J. 18, 122–127.

NACE, 2008. SP0208-2008, Internal Corrosion Direct Assessment Methodology for Liquid Petroleum. Pipelines. NACE, Houston TX.

Nädler, M., Mewes, D., 1997. Flow induced emulsification in the flow of two immiscible liquids in horizontal pipes. Int. J. Multiph. Flow 23, 55–68.

Nešić, S., 2007. Key issues related to modelling of internal corrosion of oil and gas pipelines – a review. Corros. Sci. 49, 4308–4338.

Paolinelli, L.D., Yao, J., Rashedi, A., 2017. Phase wetting detection and water layer thickness characterization in two-phase oil-water flow using high frequency impedance measurements. J. Petrol. Sci. Eng. 157, 671–679.

Perera, K., Pradeep, C., Mylvaganam, S., Time, R.W., 2017. Imaging of oil-water flow patterns by electrical capacitance tomography. Flow Meas. Instrum. 56, 23–34.

Pots, B.F.M., Hollenberg, J.F., Hendriksen, E.L.J.A., 2006. What are the Real Influences of Flow on Corrosion?, NACE Corrosion 2006. NACE, Houston, TX, Paper, p. 6591.

Pouraria, H., Seo, J.K., Paik, J.K., 2016. A numerical study on water wetting associated with the internal corrosion of oil pipelines. Ocean Eng. 122, 105–117.

Redon, C., Brochard-Wyart, F., Rondelez, F., 1991. Dynamics of dewetting. Phys. Rev. Lett. 66, 715–718.

Richter, S., Babic, M., Tang, X., Robbins, W., Nesic, S., 2014. Categorization of Crude Oils Based on Their Ability to Inhibit Corrosion and Alter the Steel Wettability, NACE Corrosion 2014. NACE, Houston, TX, Paper, p. 4247.

Schiller, L., Naumann, A., 1933. Uber die grundlegenden Berechnungen bei der Schwekraftaubereitung. Zeitschrift des Vereines Deutscher Ingenieure 77, 318–320.

Segev, A., 1984. Mechanistic Model for Estimating Water Dispersion in Crude Oil Flow. Annual AIChE Meeting, AIChE, San Francisco, CA, Paper, p. 124a.

Sleicher, C.A., 1962. Maximum stable drop size in turbulent flow. AIChE J. 8, 471–477.

Smith, S.N., Joosten, M.W., 2006. Corrosion of Carbon Steel by H_2S in CO_2 Containing Oilfield Environments, NACE Corrosion 2006. NACE, Houston, TX, Paper, p. 6115.

Srinivasan, S., McKinley, G.H., Cohen, R.E., 2011. Assessing the accuracy of contact angle measurements for sessile drops on liquid-repellent surfaces. Langmuir 27, 13582–13589.

Tang, X., 2011. Effect of Surface State on Water Wetting and Carbon Dioxide Corrosion in Oil-water Two-phase Flow. PhD thesis, Department of Chemical and Biomolecular Engineering. Ohio University, Athens, OH.

Torres, C.F., Mohan, R.S., Gomez, L.E., Shoham, O., 2015. Oil-water flow pattern transition prediction in horizontal pipes. J. Energy Res. Technol. 138, 022904-1–022904-11.

Trallero, J.L., 1995. Oil-Water Flow Patterns in Horizontal Pipes. PhD thesis, University of Tulsa, Tulsa, OK.

Trallero, J.L., Sarica, C., Brill, J.P., 1997. A study of oil-water flow patterns in horizontal pipes. SPE Product. Facilit. 12, 165–172.

Tsahalis, D.T., 1977. Conditions for the Entrainment of Settled Water in Crude Oil and Product Pipelines, 83rd National Meeting of the AIChE. AIChE, Houston, TX.

Utvik, O.H., Rinde, T., Valle, A., 2001. An experimental comparison between a recombined hydrocarbon-water fluid and a model fluid system in three-phase pipe flow. J. Energy Res. Technol. 123, 253–259.

Valle, A., 2000. CO_2 Corrosion and Water Distribution Two Phase Pipe Flow of Hydrocarbon Liquid and Water, NACE Corrosion 2000. NACE, Houston TX, Paper, p. 47.

Vielma, M.A., Atmaca, S., Sarica, C., Zhang, H.-Q., 2008. Characterization of oil/water flows in horizontal pipes. SPE Projects Facilit. Construct. 3, 1–21.

Wicks, M., Fraser, J.P., 1975. Entrainment of water by flowing oil. Mater. Perform. 14, 9–12.

Yan, J.-F., Sáez, A.E., Grant, C.S., 1997. Removal of oil films from stainless steel tubes. AIChE J. 43, 251–259.